INTERNATIONAL JOURNAL OF HYDROGEN ENERGY 40 (2015) 9621–9633

Available online at www.sciencedirect.com

ScienceDirect

journal homepage: www.elsevier.com/locate/he

Iron ore reduction by methane partial oxidation in a porous media

Pablo Palacios [a], Mario Toledo [a,*], Manuel Cabrera [b]

[a] Department of Mechanical Engineering, Universidad Técnica Federico Santa María, Av. España 1680, Valparaíso, Chile

[b] Department of Metallurgical and Materials Engineering, Universidad Técnica Federico Santa María, Av. España 1680, Valparaíso, Chile

ARTICLE INFO

Article history:
Received 31 January 2015
Received in revised form
7 May 2015
Accepted 8 May 2015
Available online 22 June 2015

Keywords:
Iron ore
Direct reduction
Methane partial oxidation
Porous media
Numerical

ABSTRACT

In this work, iron ore reduction by the gaseous products of methane partial oxidation in a porous media (H_2 and CO) is studied numerically and experimentally. A new fixed-bed reactor was designed to perform the reduction tests, along with the development of a mathematical model that considers reduction reactions, mass balance and energy equations for both gas and solid phases. The experimental results show a low reduction degree at equivalence ratio (φ) of 1.2 and allow model parameterization. The model was applied to sensitivity analyses regarding to operation parameters such as equivalence ratio and iron ore pellets size. The performed analysis predicts favorable metallization degree for high equivalence ratios (or high H_2 and CO concentrations) and smaller pellets.

Introduction

Direct reduced iron (DRI) industry has grown steadily during the last 40 years, contributing around 7% of the world's total iron-making capacity. This growth was stimulated by a desire or necessity to use lower grade ores and fuels that are unsuitable for blast furnaces [1]. In parallel with this situation, environmental friendly technologies are highly valued by society and industry, which makes necessary finding combustion processes that are more efficient than conventional ones, among which combustion in porous media arises as a very attractive alternative. This technology is characterized by being capable to burn an excessively rich or lean fuel mixture, due to the intense heat exchange between the solid media and the premixed gas fuel. Because of the heat recirculation inside the porous media, which produces an excess of enthalpy in the reaction zone, these burners have a wide range of combustion, while conventional burners do not. The transient system involves a traveling wave representing unsteady combustion zone freely propagating in either downstream or upstream direction inside the porous media. The wave velocity measurements are based on displacement of thermal profile along the reactor length. The relatively high thermal emissions with low emissions of CO and NO_x in lean mixtures

* *Corresponding author*. Tel.: +56 32 2654162; fax: +56 32 2797472.
E-mail address: mario.toledo@usm.cl (M. Toledo).
http://dx.doi.org/10.1016/j.ijhydene.2015.05.058

and excellent flame stability are basic requirements to generate industrial applications. One of the main uses of this technology is the partial oxidation of fuels utilizing a highly rich mixture [2,3]; this is done to obtain syngas ($H_2 + CO$) in the combustion products, which are the same reducing gases that DRI processes use in order to reduce the iron ore.

There are few proposed models for fixed-bed iron ore reduction reactors. Aguilar et al. [4] proposed a model of this kind based on unsteady state condition. Parisi and Laborde [5] proposed a model for a countercurrent moving bed reactor. The model considers global reduction reactions and it was validated with data available from two DRI plants. Takenaka et al. [6] proposed a shaft furnace model where reaction rate equations were derived from the three-interface model, including heat and mass balances. Alamsari et al. [7] proposed a model for a countercurrent moving bed reactor, where the three-interface model was also considered. Methane reforming and water gas shift reactions were included as the reactions that occur in the gaseous phase. The model also included heat and mass balances. Mondal et al. [8] proposed a kinetic model using CO as the reducing agent. Kinetics constants were derived based on Arrhenious equation and cementite formation reaction was considered. Valipour [9] proposed a non-isothermal model based upon a special application of the grain model, where each grain is reduced according to the unreacted shrinking core model at three-interfaces simultaneously, and included heat and mass balances. Nouri et al. [10] proposed grain model that considers the global reduction reaction by CO and H_2. The countercurrent moving bed reactor was modeled under steady state conditions. The results were contrasted with available data from a DRI plant. The kinetics of the reduction reactions is very important to develop a mathematical model of the reduction zone. Unreacted shrinking core model (USCM) proposed by Levenspiel [11] is vastly used for kinetics model of iron ore reduction in which the reaction occurs first at the outer surface of the particle. According to the model, the reaction zone then moves towards the center of the solid, leaving behind converted material and inert solid (ash). Therefore, at any time, there exists an unreacted core of reactant solid that is shrinking in size during the reaction.

The aim of this work is to perform an experimental and numerical study of the reduction of iron ore by the product gases of partial combustion of a methane-air mixture in a porous media burner, where the combustion front propagates through the iron ore bed. While porous media burners have been used in the past to produce syngas efficiently, it has not been studied its application in mineral reduction. A porous media burner is considered a fixed-bed reactor for this purpose, while most DRI industrial applications consider moving-bed reactors. In addition, when used to produce syngas, porous media burners have the capability to control the combustion wave speed adjusting the equivalence ratio.

In order to do this, a new porous media reactor was designed and built to perform the experimental tests. For the development of the mathematical model, mass balance and energy equations were taken into account, and the global reduction reactions were considered. The model was parameterized with experimental data obtained.

Experimental apparatus and procedure

Experiments on iron reduction were conducted using the setup shown in Fig. 1. The system consisted of a combustion tube filled with a porous medium, natural gas and air supply systems, a temperature measurement system, and a gas chromatograph. There were two configurations of the porous medium: In the first case, the reactor was filled with alumina spheres only, this was done with the purpose of establishing a baseline. In the second case, the porous medium was composed of two sections of alumina spheres and a section of iron ore pellets. The configuration was the following: from the reactor top to bottom, a 100 mm section filled with alumina spheres, to ensure stable initiation of upstream waves; an intermediate section filled with 120 mm of iron ore pellets. This section constitutes the reduction zone; a 40 mm section filled with alumina spheres, from the bottom of the reduction zone to the reactor bottom.

The irregular geometry of iron ore pellets was approximated by a sphere with 5 mm diameter. The specified volumes of 5.6 mm solid alumina balls and 5 mm iron ore pellets resulted in two packed beds with a porosity of ~40%. Combustion tube was made of quartz with an inner diameter of 41 mm, a wall thickness of 2 mm, and length of 30.2 cm. To avoid heat losses, to achieve quasi-uniform system temperature profiles, and to protect quartz tube, the inner surface of the combustion tube was covered with a 3 mm layer of Fiberfrax insulation and 6 mm thick high-temperature insulation was applied on the external diameter of the reactor. Combustible mixtures of natural gas with air were set up by a continuous flow method where the fuel and air flows were metered using a set of Aalborg mass flow controllers. The composition of the natural gas was 94.1% CH_4, 4.8% C_2H_6 and 1.1% of other gases. Before the reactants enter the combustion tube, they were premixed in a mixing chamber to ensure uniform gas composition. Then, the mixture was introduced through a distribution grid at the reactor bottom. The exit of the reactor was open to atmosphere. During the experiments, the upstream propagating combustion wave was initiated at the reactor exit. The upstream propagation was recorded. As the wave reached the bottom alumina section, the flame was turned off.

A ceramic shell of 0.5 cm in diameter was positioned axially in the combustion tube. It contained 0.08 cm diameter holes with three S-type (platinum/rhodium) thermocouples fabricated by OMEGA. The voltages measured by the thermocouples were recorded by an OMB DAQ 54 acquisition module and converted by the Personal DaqView Software. The thermocouple junctions were spaced 6 cm apart along the length of the shell. The first one was located at 7 cm below the reactor exit. The thermocouples were completely covered by the ceramic shell allowing to record temperatures very close to solid phase temperatures. The axial position of the thermocouples provided minimal disturbances to the gas flow and heat fluxes in the reaction zone. The experimental error in the temperature measurements was estimated as ~50 K and the error in the flow measurements was ~10%. To measure the exhaust gas composition a PerkinElmer gas chromatograph, model CLARUS 500, was used. The gas samples were taken

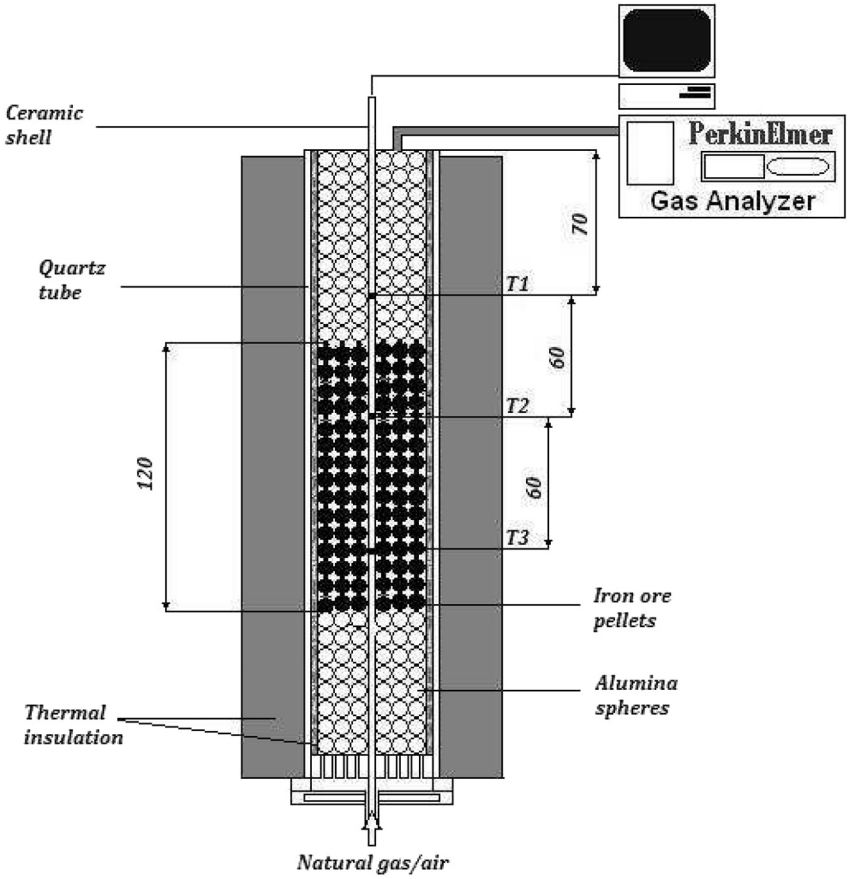

Fig. 1 – Schematic of the experimental setup.

through a Pyrex tube which was introduced 3 cm inside of the porous media at the exit of the reactor. The other end of the tube was connected to a gas sampling bag. The suction sampling was performed through a vacuum pump connected to a two-valve system that was also designed for purging the gas line and the gas sampling bag. The sample was introduced in the gas chromatograph via a 1 ml syringe. The accuracy of chemical sampling was close to 15%.

Numerical model

The numerical analyzing consisted of two parts: simulating the partial oxidation of methane in an inert porous media, and modeling the reduction of iron ore. The virtual reactor is shown in Fig. 2. The model used for the partial oxidation of methane, that is, the generation of the reducing agents H_2 and CO, was the same that Toledo et al. [12] proposed, which describes a fully developed steady combustion wave in a system of coordinates moving with the reaction zone. In Toledo's work, the GRI 3.0, an extensively validated chemical kinetic mechanism with inclusive NO_x chemistry, was used along with the Chemkin package of corresponding subroutines and databases, using a modified version of the PREMIX algorithm.

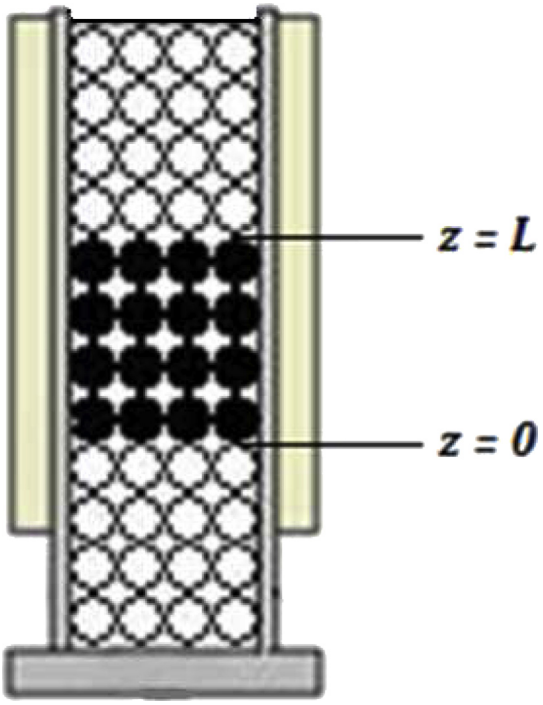

Fig. 2 – Inlet and exit of the virtual reactor.

In order to model the reduction of iron ore in a fixed-bed reactor, the following approximations were considered: (i) unsteady-state operation is assumed and the reduction reactor is considered to be one-dimensional, (ii) only the global reduction reactions are taken into account, (iii) the reducing agents are both hydrogen and carbon monoxide, which are present in gaseous mix that behaves as an ideal gas, (iv) the composition of the reducing gas was obtained simulating the partial combustion of methane in the modified PREMIX code, using GRI-Mech 3.0 and the Chemkin package, and its value is considered constant at the beginning of the reduction zone (z = 0), (v) physical and chemical properties of the species involved are depending of temperature, (vi) an isobaric, non-isothermic, two-temperature model approach is assumed, (vii) axial and radial dispersion are neglected, (viii) the irregular geometry of the iron ore pellets is approximated by spheres with a 5 mm diameter, and its consumption is governed by the unreacted shrinking core model, (ix) pellets are considered as porous solids for mass transfer effects, and as fully dense solids for heat transfer effects, (x) mass diffusion of the products is neglected compared to the heat transfer that occurs inside the reactor, and (xi) product gases do not react with the iron ore.

The reaction system studied is the following:

$$\frac{1}{3}Fe_2O_3 + H_2 \rightarrow \frac{2}{3}Fe + H_2O \tag{1}$$

$$\frac{1}{3}Fe_2O_3 + CO \rightarrow \frac{2}{3}Fe + CO_2 \tag{2}$$

It must be noted that water gas shift reaction, which is a very important reaction in iron reduction processes, is a linear combination of reactions (1) and (2).

Under the above assumptions (i) - (xi), mass balance equations for the gaseous and solid phases can be stated as:

- Gas phase:

$$\frac{\partial C_{H_2}}{\partial t} + u_g\frac{\partial C_{H_2}}{\partial z} = n_p \cdot r_{H_2}(C_{H_2}, T_s) \tag{3}$$

$$\frac{\partial C_{CO}}{\partial t} + u_g\frac{\partial C_{CO}}{\partial z} = n_p \cdot r_{CO}(C_{CO}, T_s) \tag{4}$$

- Solid phase:

$$\frac{\partial C_{Fe_2O_3}}{\partial t} = n_p \cdot r_{Fe_2O_3}(C_{H_2}, C_{CO}, T_s) \tag{5}$$

By taking averages over an elemental volume of the medium, the energy equations for both phases can be presented in the following form [13]:

- Gas phase:

$$\varepsilon(\rho C_p)_g\left(\frac{\partial T_g}{\partial t} + u_g\frac{\partial T_g}{\partial z}\right) = \frac{\partial}{\partial z}\left(\varepsilon\lambda_g\frac{\partial T_g}{\partial z}\right) + h_v(T_s - T_g) + \dot{Q}_v \tag{6}$$

- Solid phase:

$$(1-\varepsilon)(\rho C_p)_s\frac{\partial T_s}{\partial t} = \frac{\partial}{\partial z}\left(\lambda_{ef}\frac{\partial T_s}{\partial z}\right) + h_v(T_g - T_s) - \beta_v(T_s - T_0) + (1-\varepsilon)n_p\sum_{j=1}^{2}\Delta H_j r_j \tag{7}$$

The initial conditions of the proposed model are:

$$\begin{aligned} &t = 0: \quad C_{H_2} = C^0_{H_2}, C_{CO} = C^0_{CO},\ C_{Fe_2O_3} = C^0_{Fe_2O_3} \\ &T_s = T_g = T_0 \end{aligned} \tag{8}$$

And the boundary conditions are:

$$\begin{aligned} &z = 0: \quad C_{H_2} = C^0_{H_2}, C_{CO} = C^0_{CO}, C^{n+1}_{Fe_2O_3} = C^n_{Fe_2O_3}, T_g = T_s = T_0 \\ &z = L: \quad \frac{\partial C_{H_2}}{\partial z} = \frac{\partial C_{CO}}{\partial z} = \frac{\partial C_{Fe_2O_3}}{\partial z} = \frac{\partial T_s}{\partial z} = \frac{\partial T_g}{\partial z} = 0 \end{aligned} \tag{9}$$

The kinetic equations of iron ore reduction are obtained based on the shrinking core model for spherical particles of unchanging size presented by Levenspiel [11], where the reduction reaction occurs in 5 steps. Considering the property of combination of resistances, the reaction rate expressions per pellet are given by:

- Fe_2O_3:

$$-r_{Fe_2O_3} = A_p b\left(\frac{\zeta C_{CO}}{\frac{1}{k_{CO}} + \frac{R(R-r_c)}{r_c\mathscr{D}_{e,co}} + \frac{R^2}{r_c^2 k''_{CO}}} + \frac{\xi C_{H_2}}{\frac{1}{k_{H_2}} + \frac{R(R-r_c)}{r_c\mathscr{D}_{e,H_2}} + \frac{R^2}{r_c^2 k''_{H_2}}}\right) \tag{10}$$

- CO:

$$-r_{CO} = \frac{\zeta A_p C_{CO}}{\frac{1}{k_{CO}} + \frac{R(R-r_c)}{r_c\mathscr{D}_{e,co}} + \frac{R^2}{r_c^2 k''_{CO}}} \tag{11}$$

- H_2:

$$-r_{H_2} = \frac{\xi A_p C_{H_2}}{\frac{1}{k_{H_2}} + \frac{R(R-r_c)}{r_c\mathscr{D}_{e,H_2}} + \frac{R^2}{r_c^2 k''_{H_2}}} \tag{12}$$

Where $A_p = 4\pi R^2$ is the pellet surface area. Equation (10) considers a combination of resistances which include diffusion through the gas film, diffusion through the ash layer and the chemical reaction. A detailed derivation of these equations can be found in Refs. [7] and [11]. Mass transfer coefficients between fluid and particle (k_{CO}&k_{H_2}) and first-order rate constants for the surface reactions (k''_{CO}&k''_{H_2}) are calculated based on Parisi and Laborde [5] work as:

$$k_{H_2} = k''_{H_2} = 0.00225e^{\left(-\frac{14700}{82.06\ T_s}\right)} \tag{13}$$

$$k_{co} = k''_{CO} = 0.00650\,e^{\left(-\frac{28100}{82.06\ T_s}\right)} \tag{14}$$

While effective diffusion coefficient is calculated based on Alamsari et al. [7] work as:

$$\mathscr{D}_{e,\ CO\ o\ H_2} = \frac{\varepsilon_p\mathscr{D}_{M,CO\ or\ H_2-Gas}}{\tau_p} \tag{15}$$

Molecular diffusion is calculated using the Fuller-Schettler-Giddings equation [14]:

$$\mathscr{D}_{M,CO\ or\ H_2-Gas} = \frac{10^{-7}T^{1.75}}{P\left[\left(\sum\overline{v}_{CO\ or\ H_2}\right)^{\frac{1}{3}} + \left(\sum\overline{v}_g\right)^{\frac{1}{3}}\right]^2}\left(\frac{1}{M_{CO\ or\ H_2}} + \frac{1}{M_g}\right)^{\frac{1}{2}} \tag{16}$$

ζ and ξ are adjustment factors that account for more precise values of k_i and k''_i.

Considering the unreacted core model, it is possible to relate the radius of the unreacted core (r_c) with the solid conversion (Co) by Ref. [5]:

$$r_c = \left(R^3 - \frac{Co \cdot M_{Fe_2O_3}}{n_p \cdot 4\pi \cdot \rho_{Fe_2O_3}}\right)^{1/3} \quad (17)$$

Where:

$$Co = 3 \cdot \left(C^0_{Fe_2O_3} - C_{Fe_2O_3}\right) \quad (18)$$

Metallization degree is calculated using:

$$Met = \frac{Co}{3C^0_{Fe_2O_3}} \quad (19)$$

Thermophysical properties of the gaseous phase, i.e. gas conductivity, viscosity, heat capacity and density, were obtained from Toledo [15] and are calculated as follows:

$$C_{p,g} = 947.0\, e^{1.83 \cdot 10^{-4}\, T_g} \quad (20)$$

$$\lambda_g = 4.82 \cdot 10^{-7}\, C_{p,g}\, T_g^{0.7} \quad (21)$$

$$\mu_g = 3.37 \cdot 10^{-7}\, T_g^{0.7} \quad (22)$$

$$\rho_g = \frac{P \cdot M_g}{R_u \cdot T_g} \quad (23)$$

The specific heat, thermal conductivity and density of the solid phase were estimated as follows [5]:

$$C_{p,s} = \frac{C_{p,Fe_2O_3}\rho_{Fe_2O_3} r_c^3 + C_{p,Fe}\rho_{Fe}\left(R^3 - r_c^3\right)}{\rho_{Fe_2O_3} r_c^3 + \rho_{Fe}\left(R^3 - r_c^3\right)} \quad (24)$$

$$\lambda_s = \frac{\lambda_{Fe_2O_3}\rho_{Fe_2O_3} r_c^3 + \lambda_{Fe}\rho_{Fe}\left(R^3 - r_c^3\right)}{\rho_{Fe_2O_3} r_c^3 + \rho_{Fe}\left(R^3 - r_c^3\right)} \quad (25)$$

$$\rho_s = \frac{\rho_{Fe_2O_3} r_c^3 + \rho_{Fe}\left(R^3 - r_c^3\right)}{R^3} \quad (26)$$

The volumetric convective heat transfer coefficient is found as [12]:

$$h_v = \frac{6(1-\varepsilon)}{D^2}\lambda_g Nu \quad (27)$$

The correlation for Nusselt is given by Wakao and Kaguei [16] as:

$$Nu = 2 + 1.1 Pr^{1/3} Re^{0.6} \quad (28)$$

Radiation is treated with radiant conductivity model, where both effective thermal conductivity and radiation are included in the overall conductivity of the porous media, which is given by Toledo [15] as:

$$\lambda_e = 0.005\lambda_s + 4\sigma D T_s^3 \frac{\varepsilon}{1-\varepsilon} \quad (29)$$

Bed porosity was estimated as 40%. Heat transfer coefficient to the surroundings is given by Toledo [15] as:

$$\beta_v = \frac{4}{D_c}\left(h + \varepsilon' \cdot \varepsilon'' \cdot \sigma \cdot \frac{T_s^4 - T_0^4}{T_s - T_0}\right) \quad (30)$$

Where h was estimated as 10 [W/m^{2}K].

The expression $\sum_{j=1}^{2} \Delta H_j r_j$ in equation (7) makes reference to the heat of reduction reactions (1) and (2). The formulation is described as follows:

$$\sum_{j=1}^{2} \Delta H_j r_j = \Delta H_{red,\,CO} r_{CO} + \Delta H_{red,\,H_2} r_{H_2} \quad (31)$$

$$\Delta H_{red,CO}(T_s) = \left[\frac{2}{3}\left(\Delta H^0_{f,Fe} + \int_{T_0}^{T_s} C_{p,Fe}\, dT\right) + \left(\Delta H^0_{f,CO_2} + \int_{T_0}^{T_s} C_{p,CO_2}\, dT\right)\right] - \left[\frac{1}{3}\left(\Delta H^0_{f,Fe_2O_3} + \int_{T_0}^{T_s} C_{p,Fe_2O_3}\, dT\right) + \left(\Delta H^0_{f,CO} + \int_{T_0}^{T_s} C_{p,CO}\, dT\right)\right] \quad (32)$$

$$\Delta H_{red,H_2}(T_s) = \left[\frac{2}{3}\left(\Delta H^0_{f,Fe} + \int_{T_0}^{T_s} C_{p,Fe}\, dT\right) + \left(\Delta H^0_{f,H_2O} + \int_{T_0}^{T_s} C_{p,H_2O}\, dT\right)\right] - \left[\frac{1}{3}\left(\Delta H^0_{f,Fe_2O_3} + \int_{T_0}^{T_s} C_{p,Fe_2O_3}\, dT\right) + \left(\Delta H^0_{f,H_2} + \int_{T_0}^{T_s} C_{p,H_2}\, dT\right)\right] \quad (33)$$

Values of standard enthalpies of formation (ΔH^0_f) and specific heats (C_p) were taken from NIST webpage [17]. $\dot{Q}_v$, the heat generation due to the unconsidered reactions that occur in the gaseous phase, was treated as a parameter of the model. The most important unconsidered reactions are:

Water Gas Shift Reaction:

$$H_2O + CO \rightarrow CO_2 + H_2 \quad (34)$$

Boudouard Reaction:

$$2CO \leftrightarrow CO_2 + C \quad (35)$$

Methanation Reaction:

$$CO + 3H_2 \rightarrow CH_4 + H_2O \quad (36)$$

The differential equations system (3)–(7) with initial and boundary conditions (8) and (9) was solved numerically using the tri-diagonal matrix algorithm. Parameters ζ, ξ and $\dot{Q}_v$ were adjusted to experimental data.

Results and discussion

Results are presented in two sections: the first section contains the experimental results of both the experimental baseline and the iron ore reduction tests; the second part contains the numerical results obtained with the iron ore reduction model.

In order to obtain the experimental baseline, the equivalence ratio, defined as the ratio between stoichiometric air flow and real air flow must be calculated. The stoichiometric volume of air needed to burn a kilogram of fuel at normal temperature and pressure conditions is given by:

$$V_{a,st} = \frac{22.39}{X_{O_2}}\left(\frac{y_C}{12.01} + \frac{y_H}{4.032}\right)\left[\frac{Nm^3 air}{kg\ fuel}\right] \quad (37)$$

Where y_C and y_H are defined as the mass fractions of carbon and hydrogen in the fuel, in this case natural gas, and X_{O_2} is the volume fraction of oxygen in the air. Thus, the stoichiometric air flow is calculated as:

$$\dot{V}_{a,st} = V_{a,st} \cdot \dot{m}_f$$
$$\dot{V}_{a,st} = V_{a,st} \cdot \rho_f \cdot \dot{V}_f \quad (38)$$

Where ρ_f, fuel density, is obtained considering normal temperature and pressure conditions. The equivalence ratio, φ, is given by:

$$\varphi = \frac{\dot{V}_{a,st}}{\dot{V}_{a,real}} \quad (39)$$

In the experimental setup, $\dot{V}_{a,real}$ and $\dot{V}_f$, real air flow and fuel flow respectively, were adjusted manually to obtain the desired equivalence ratio. Equivalence ratio can be interpretated as follows:

- $\varphi < 1$ indicates a lean air-natural gas mixture.
- $\varphi = 1$ indicates stoichiometric mixture.
- $\varphi > 1$ indicates a rich air-natural gas mixture.

The experimental baseline contains the data obtained for natural gas-air mixtures inside alumina spheres-only porous media at three filtration velocities of 18, 22 and 25 cm/s at an equivalence ratio of $\varphi = 1.2$. The iron ore reduction tests were carried out at a filtration velocity of 22 cm/s and at equivalence ratios of $\varphi = 1.1$ and $\varphi = 1.2$. In all the cases, the solid phase temperature, H_2, CO and CO_2 concentrations in the exhaust were measured. The propagation rates were obtained from the thermocouple traces. In addition to this, atomic absorption spectroscopy (AAS) and X-Ray diffraction (XRD) analyses were performed to verify if the iron ore was reduced after the tests.

The numerical results obtained with the modified PREMIX algorithm were used to obtain some of the initial and boundary conditions of the iron ore reduction model. The reduction model was parameterized with experimental data obtained for $\varphi = 1.2$. Sensitivity analyses were performed to the model regarding total simulation time, equivalence ratio and pellets size.

Experimental results

Table 1 shows the results obtained for filtration velocities of 19, 22 and 25 cm/s. To ensure a stable initiation of the propagation wave and to prevent the melting of the iron ore due to the high temperatures reached inside the reactor, the filtration velocity selected for the reduction tests was 22 cm/s.

Table 1 – Temperature results obtained for the experimental baseline with different filtration velocities, $\varphi = 1.2$.

Filtration velocity (cm/s)	Temperature (K)	Wave propagation rate (cm/s)
19	1079	−0.0054
22	1116	−0.0074
25	1404	−0.0102

Table 2 shows the results obtained for the iron ore reduction tests conducted. Two tests were carried out: one with $\varphi = 1.1$ and one with $\varphi = 1.2$. For this configuration of the reactor, the propagation waves were extinguished at equivalence ratios higher than 1.2. For an equivalence ratio of 1.2, temperatures reached inside of the iron ore porous media were significantly higher than those reached inside the alumina spheres (~300 K). This can be explained due to the predominant reactions that occur in the reaction zone are exothermic, namely both hematite to magnetite reduction reactions with CO and H_2 as reducing agents, where the reduction reaction with CO is more exothermic than the one with H_2 [18]. Another explanation for the increase of the temperature is found in the reactions that occur in the gaseous phase, namely water gas shift reaction, CO disproportionation and methanation reaction, which are all exothermic. The slower wave propagation rate in the reduction tests can be explained due to the physical properties of the iron ore, and the different kind of reactions that occur in each porous medium.

Table 3 shows a comparison of the concentrations of the main measured combustion products for both the baseline (partial oxidation of natural gas) and the iron ore reduction tests. The lower concentration of CO and H_2, plus the higher concentration of CO_2 in the reduction tests are clear signals that the iron ore was reduced in some amount during the tests. The lower concentration of CO compared to H_2 can be explained by the reactions that occur in the gaseous phase, mainly water gas shift reaction, and CO disproportionation in a lesser extent. The higher concentration of CH_4 can be explained due to methanation reaction, which uses iron oxide as a catalyst.

The hydrogen and carbon monoxide conversion are calculated using the initial hydrogen and carbon content in natural gas (methane). The yields recorded were 42.8% and 89.3% for the baseline (Table 3).

In addition, other analyses were performed to prove that the iron ore was reduced using this specific reactor configuration. X-Ray diffraction analyses were made for the unreacted iron ore and the reduced iron ore with $\varphi = 1.1$ and $\varphi = 1.2$. Results are shown in Table 4 and Table 5 and the diagrams are shown in Figs. 3–5. The unreacted iron ore was composed mainly by Fe_2O_3, whether it is hematite or maghemite. Pellets are formed from magnetite ore, so the presence of maghemite can be explained due to the oxidation process that occurs when the pellets are produced. Reduction test with $\varphi = 1.1$ showed the presence of the three main iron oxides, but it didn't show the presence of metallic iron. Thus, the metallization degree reached was very low or null. Nonetheless, the

Table 2 – Temperature results obtained for the iron reduction tests, filtration velocity of 22 cm/s.

φ	Temperature (K)	Wave propagation rate (cm/s)
1.1	1518	−0.0013
1.2	1409	−0.0019

Table 3 – Comparison between baseline tests and iron reduction tests regarding product gases concentration and methane conversion, filtration velocity of 22 cm/s, $\varphi = 1.2$.

Test performed	$\%H_2$	%CO	$\%CH_4$	$\%CO_2$	% $H_2/(2*CH_{4,inlet})$ Conversion	% $CO/CH_{4,inlet}$ conversion
Baseline	9.5	9.9	0.7	3.9	42.8	89.3
Iron ore reduction	2.9	1.6	2.4	15.3	13.1	14.4

Table 4 – XRD results of the unreacted iron ore.

Specie	Chemical formula
Hematite	$\alpha - Fe_2O_3$
Maghemite	$\gamma - Fe_2O_3$
Chrome-Iron Oxide	$(Fe_{0.6}Cr_{0.4})_2O_3$

Table 5 – XRD results of the reduced iron ore, $\varphi = 1.1$ and $\varphi = 1.2$.

φ	Specie	Chemical formula
1.1	Hematite	$\alpha - Fe_2O_3$
	Magnetite	Fe_3O_4
	Wustite	FeO
1.2	Maghemite	$\gamma - Fe_2O_3$
	Lepidocrocite	$\gamma - FeO(OH)$
	Chrome-Iron Oxide	$(Fe_{0.6}Cr_{0.4})_2O_3$
	Magnesium–Iron Oxide	$Mg_{1-x}Fe_xO$

presence of magnetite and wustite proves that it the iron ore was reduced in some amount. Also, hematite presence can be explained because part of the iron ore didn't react. It is possible that part of the magnetite formed was due to reoxidation of wustite, and part of the hematite formed was due to reoxidation of magnetite. Reduction test with $\varphi = 1.2$ showed the presence of maghemite, lepidocrocite, Cr–Fe Oxide and Mg–Fe Oxide. The absence of magnetite, wustite and metallic iron confirms that a low degree of reduction was achieved. Maghemite presence can be explained due to reoxidation of magnetite, while lepidocrocite content can be explained due to weathering of the reduced iron ore. Cr–Fe oxide was found in the unreacted iron sample, so it is probable that it didn't react during the reduction tests.

Table 6 shows the results of the AAS analyses conducted. The iron concentration in the three samples is similar, as thus the degree of reduction achieved was low, which is in agreement with the results obtained from the XRD analyses. The expression used for the calculation of the degree of reduction is the following:

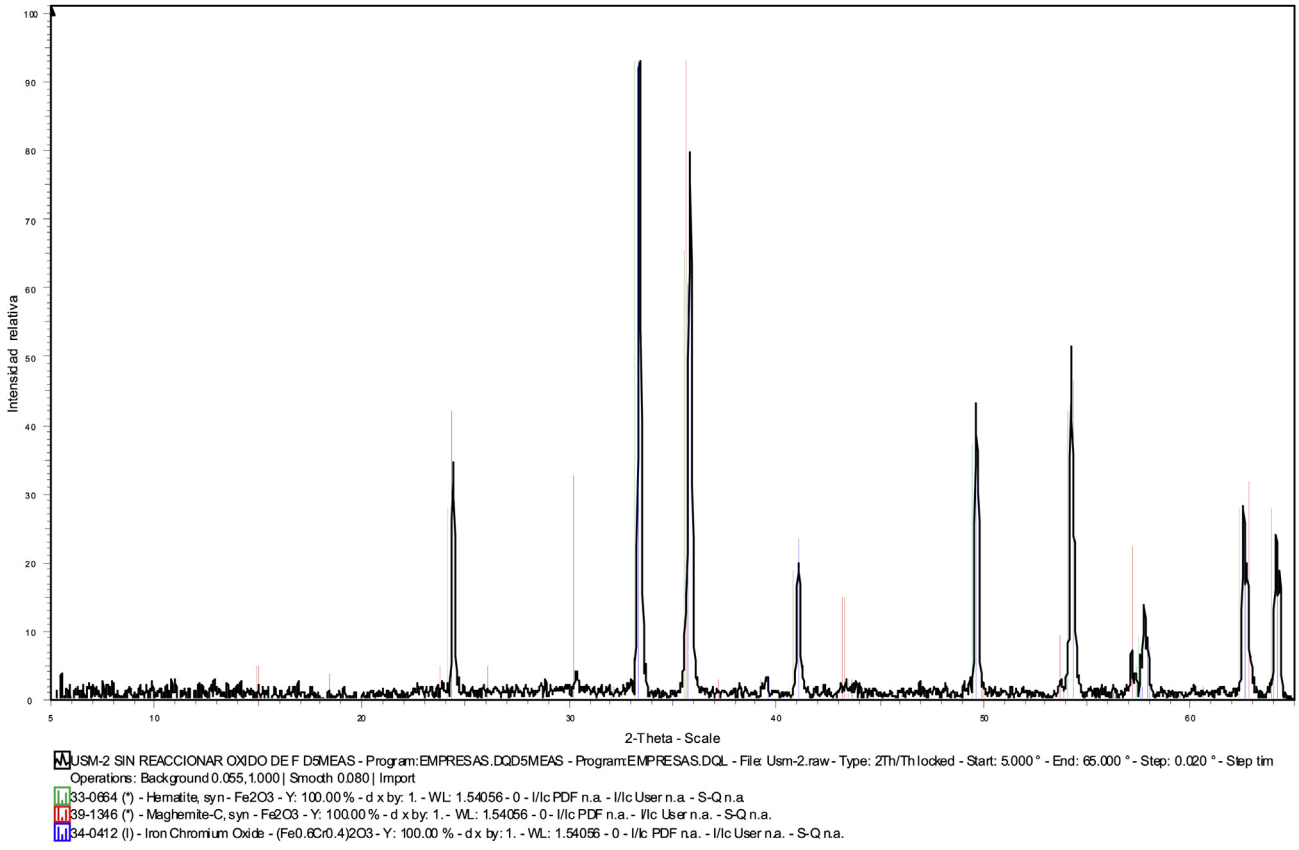

Fig. 3 – X-Ray Diffraction Diagram for the unreacted ore.

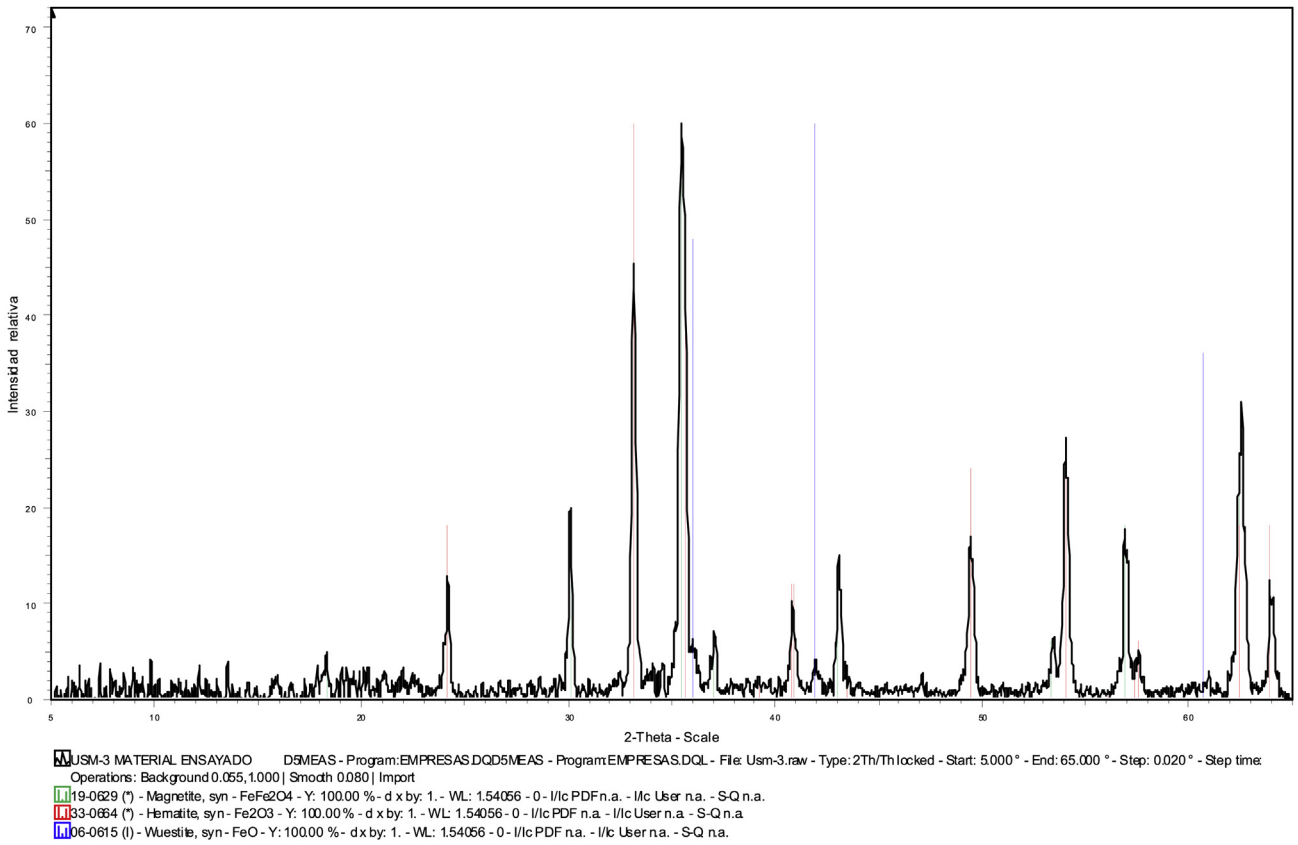

Fig. 4 – X-Ray Diffraction Diagram for the reduced iron ore, $\varphi = 1.1$.

$$Reduction = \frac{\left(\frac{\%O_2}{\%Fe_T}\right)_{\text{Iron Ore}} - \left(\frac{\%O_2}{\%Fe_T}\right)_{\text{DRI}}}{\left(\frac{\%O_2}{\%Fe_T}\right)_{\text{Iron Ore}}} \times 100 \quad (40)$$

Where:

$$Fe_T = \frac{\text{Total iron mass}}{\text{Total mass of the sample}} \times 100 \quad (41)$$

Numerical simulation results

Numerical simulation of partial oxidation of methane-air mix

As it was explained, the results obtained from the modified PREMIX algorithm were used to determine some of the initial and boundary conditions of the iron ore reduction model, namely the values of $C^0_{H_2}$ and C^0_{CO}. These results have a good agreement with the results presented by Toledo et al. [12].

Model parameterization

Due to the lack of experimental data of iron ore reduction tests in porous media burners, iron ore reduction model was parameterized with the available data of the reduction tests for an equivalence ratio of 1.2. The parameterization was carried out by comparing the concentration at the reduction zone exit and temperature of the solid phase. Table 7 shows the adjusted parameters used during the numerical simulation of the model. The total simulation time was of 40 min, where the reactor reached steady temperatures for both the solid and the gaseous phases.

The model results agree satisfactorily with the experimental data, as it is shown in Table 8. The maximum temperature of the solid phase and the temperature profile are strongly determined by the value of $\dot{Q}_v$. The difference in CO_2 yield can be explained due to unconsidered reactions that occur in the gaseous phase, like methanation reaction, CO disproportionation and water gas shift reaction.

Sensitivity analysis

Sensitivity analyses were performed to the model with the purpose of predicting the behavior of metallization degree regarding total simulation time, equivalence ratio and pellet size.

Total simulation time. Regarding the metallization degree achieved, it can be seen that this value increases with simulation time, and the mineral is converted at the reduction zone inlet first, while the reduction zone exit is the last to be fully converted. This means that reaction rates are higher in the inlet of the reduction zone, which is highly dependant of both solid phase temperature and concentration values. Metallization degree profiles are shown in Fig. 6 and overall metallization degree are presented in Table 9. It can be appreciated that for a simulation time of 120 min, the overall metallization degree achieved is about 92%, which is similar to those

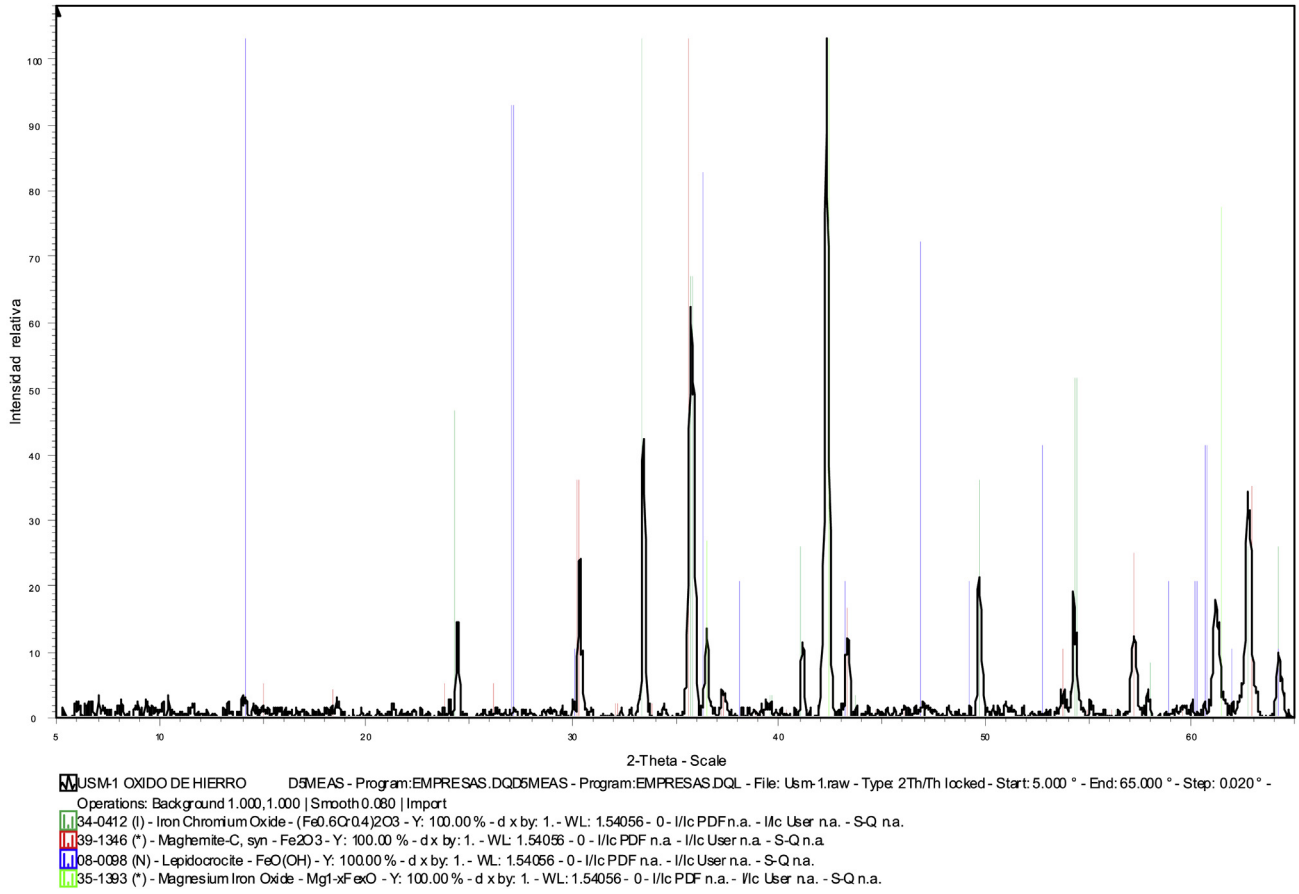

Fig. 5 – X-Ray Diffraction Diagram for the reduced iron ore, φ = 1.2.

achieved for industrial processes like HYL or MIDREX [1]. For a simulation time of 160 min, it is expected the full conversion of the iron ore.

Equivalence ratio. Fig. 7 shows the results for the maximum temperature of the solid phase reached, maximum metallization degree and overall metallization degree achieved. It can be seen that the maximum temperatures reached for the solid phase are very similar in the range of equivalence ratios simulated, where the value is close to 1414 K, which is strongly determined by the value of $\dot{Q}_v$. Regarding the metallization degrees, it can be appreciated that both values tend to increase with equivalence ratio, reaching a maximum metallization degree of 73.3% at φ = 3.75, with an overall metallization degree of 40.7%. Considering that the tendency indicates that these values would be higher at higher equivalence ratios, it can be said that using the higher possible equivalence ratio (or higher H_2 and CO concentrations) favors achieving a higher metallization degree in the least possible time. This can be explained due to the higher reaction rates, which are dependent of both the temperature and the

Table 6 – AAS results of the different iron ore samples.

Sample	(g Fe/100 g)	Average, (g Fe/100 g)	Degree of reduction %
Unreacted iron ore	Máx: 65.95 Mín: 65.30	65.62	–
Reduced iron ore, φ = 1.1.	Máx: 66.62 Mín: 66.71	66.67	4.581%
Reduced iron ore, φ = 1.2.	Máx: 66.34 Mín: 67.16	66.75	4.924%

Table 7 – Adjustment factors.

Parameter	Selected value
ζ	2.53 (–)
ξ	4.11 (–)
$\dot{Q}_v$	$1.135 \cdot 10^7$ (J/kmol)

Table 8 – Comparison between experimental data and model predictions regarding the concentration of the product gases at the reduction zone exit and maximum solid phase temperature reached.

Variable	Experimental φ = 1.2	Model φ = 1.2
Molar fraction of H_2 (%)	2.9	2.9
Molar fraction of CO (%)	1.6	1.6
Molar fraction of CO_2 (%)	15.3	12.3
Ts max (K)	1409	1414

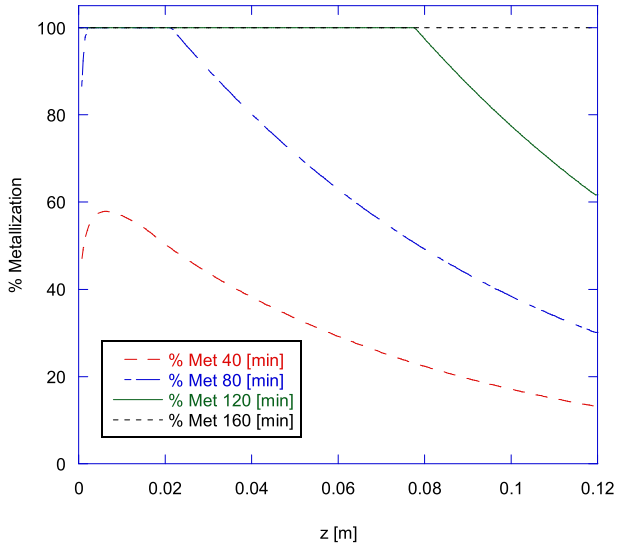

Fig. 6 – Metallization degree profile predicted for different simulation times, φ = 2.

concentrations of the reducing gases, and as it was mentioned before, they tend to increase with the equivalence ratio.

Pellet size. Concentration profiles of CO and H_2 are shown in Fig. 8. It can be appreciated that both gases are more reduced when the pellets are smaller. This can be explained because mass balance equations (3) and (4) depend, among other variables, of both the pellet area (αR^2) and the number of pellets per volume unit n_p (αR^{-3}). This means a bigger total surface area of the spheres, which favors heat transfer between solid and gas phases and a higher heat of reaction. Therefore, an increase of the pellet size implies a decrease of the concentration gradient of CO and H_2. Based on the aforementioned, metallization degree achieved is higher with smaller pellets, as it is shown in Fig. 9 and Table 10.

The model predicts that metallization degree is favored under the following conditions:

- Higher simulation time, that is, longer experiments.
- Using higher equivalence ratios.
- Using smaller pellets.

Table 9 – Overall metallization degrees achieved for different simulation times, φ = 2.

Simulation time	% Overall metallization degree
40 (min)	32.0
80 (min)	65.7
120 (min)	92.6
160 (min)	100.0

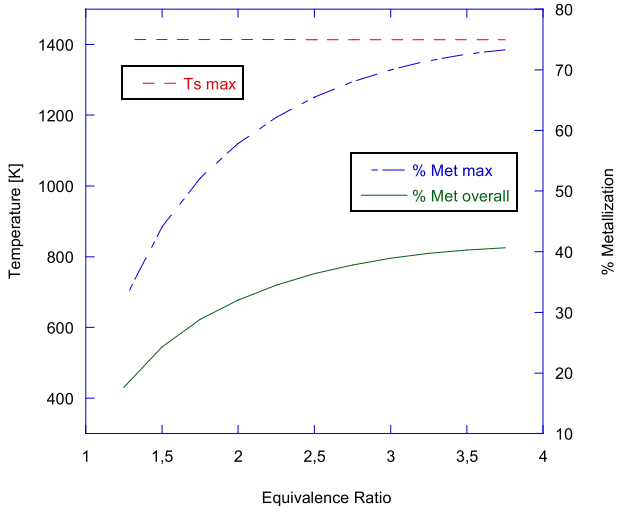

Fig. 7 – Numerical predictions obtained for the maximum temperature of the solid phase reached and the metallization degree achieved with variation of the equivalence ratio, t = 40 min.

Conclusions

Iron ore reduction by the gaseous products of partial combustion of methane in a porous media was experimentally

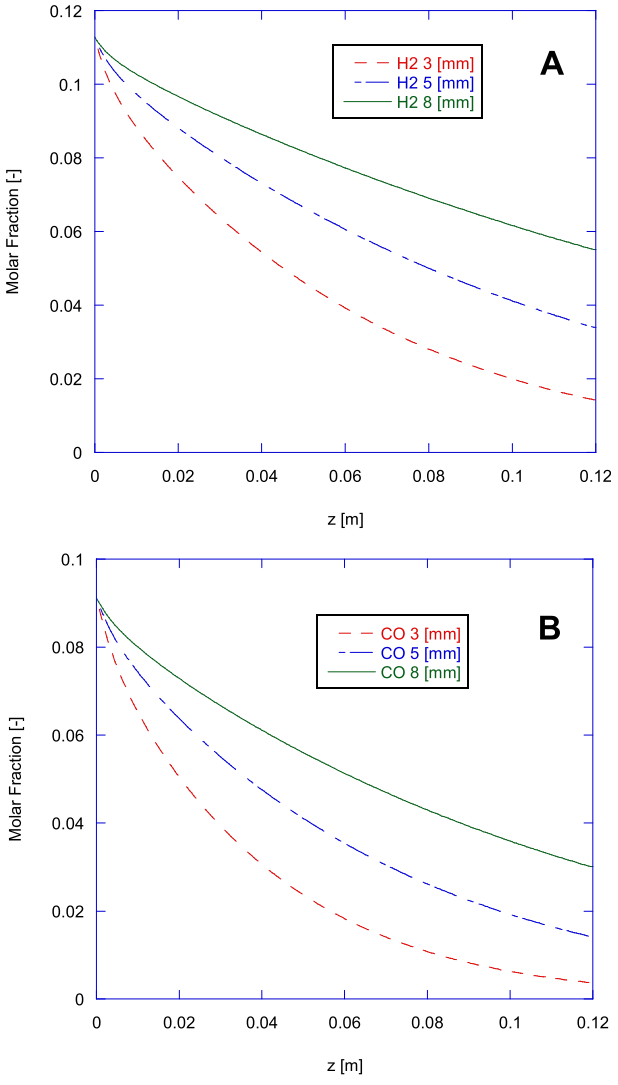

Fig. 8 – Concentration profiles of H_2 (A) and CO (B) predicted for different pellet sizes, φ = 2, t = 40 min.

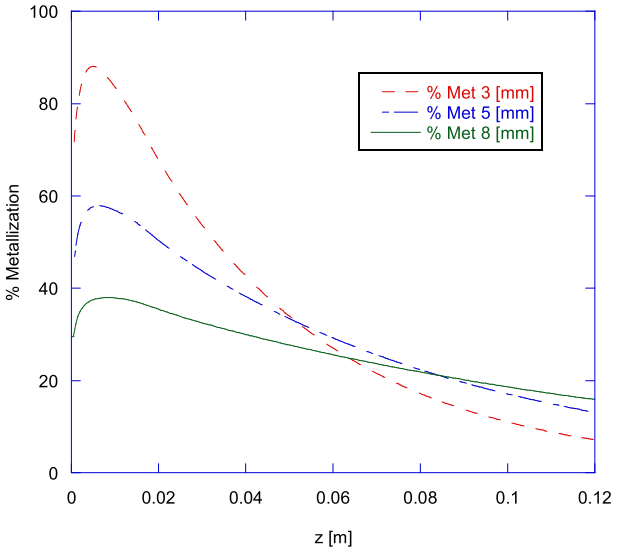

Fig. 9 – Metallization degree profile predicted for different pellet sizes, φ = 2, t = 40 min.

and numerically studied. To achieve this purpose, a porous media burner capable of generating an upstream propagation wave for the rich combustion of natural gas-air mixture was designed and built. Two experimental tests were performed, with equivalence ratios of φ = 1.1 and φ = 1.2. The iron ore reduction model was simulated in two parts: The first part, the reducing gas generation model, was simulated using the modified PREMIX algorithm with GRI-Mech 3.0 reaction mechanism along with a Chemkin package. The second part, the reduction model, was simulated considering the global reduction reaction of Fe_2O_3 to Fe, mass balance and energy equations.

Experimental results showed that the degree of reduction achieved was low. XRD analyses proved the existence of magnetite, wustite and maghemite in the reduced ores, but no metallic iron. Maghemite presence is attributed to reoxidation of previously formed magnetite, and some of the magnetite formed is due to reoxidation of wustite. AAS analyses ratified the low degree of reduction, where the total Fe content of the original sample and the reduced samples were similar.

Gas chromatography showed that both CO and H_2 concentrations in the reduction tests were significantly lower that the concentrations obtained for the experimental baseline, while CO_2 and CH_4 concentrations were higher. In addition to this, the maximum temperature reached inside the iron ore porous media was about 300 K higher than the temperature obtained for the experimental baseline. This can be explained because of the exothermic reduction reactions that occur in the iron ore, namely the reduction reactions of Fe_2O_3 to Fe_3O_4 by CO and H_2, in addition to the unconsidered exothermic reactions that occur in the gaseous phase. These reactions also explain the increase in the concentration of CH_4 and CO_2 in the products.

Reduction model was parameterized with the experimental data obtained for φ = 1.2. Model predictions have a good agreement with the experimental results regarding the solid phase temperature and concentrations of both CO and H_2. The difference in CO_2 yield can be explained due to unconsidered reactions that occur in the gaseous phase, namely methanation, CO disproportionation and water gas shift reaction.

Several sensitivity analyses were performed to the model regarding operation parameters, like total simulation time, equivalence ratio and pellet size. It was also found that for a simulation time of 2 h, the overall metallization degree achieved was 92.6%, which is close to those achieved for industrial processes. Regarding equivalence ratio, the model predicted a maximum metallization degree of 73.3% at φ = 3.75, with an overall metallization degree of 40.7% for a simulation time of 40 min. Considering that the tendency indicated that these values would be higher at higher equivalence ratios, using the higher possible equivalence ratio favors achieving a higher metallization degree in the least possible time. This can be explained due to higher reaction rates, which are dependant of both the temperature and the concentrations of the reducing gases, with the latter tending to increase with the equivalence ratio. Regarding the size of the pellets, the model predicted that CO and H_2 were more reduced when the pellets were smaller, this happens because mass balance equations depend of both the pellet area ($\propto R^2$) and the number of pellets per volume unit n_p ($\propto R^{-3}$). Also, the bigger total surface area of the spheres favors heat transfer between solid and gas phases and a higher heat of reaction. Therefore, an increase of the pellet size implies a decrease of the concentration gradient of CO and H_2. Based on the aforementioned, metallization degree achieved was higher with smaller pellets.

Future investigations should be focused in developing a porous media burner capable of producing stable propagation waves for equivalence ratios higher than 1.2 and to include a more complete reaction system, including the 3-step reduction reaction of Fe_2O_3 to Fe, and also the reactions that occur in the gas phase, as they played an important role in the reactor. This reactor configuration should include a mechanism to ensure stable initiation of downstream propagation waves. By doing this, experimental tests where the wave propagation rate is close to zero could be performed.

Table 10 – Overall metallization degrees achieved for different pellet sizes, φ = 2, t = 40 min.

Pellet diameter	% Overall metallization degree
3 (mm)	35.5
5 (mm)	32.1
8 (mm)	26.3

Acknowledgments

The authors wish to acknowledge the support of CONICYT-Chile under Fondecyt project 1121188, and DGIP of UTFSM.

REFERENCES

[1] Feinman J. In: Wakelin DH, editor. Direct reduction and smelting processes. Pittsburgh, PA: The AISE Steel Foundation; 1999. p. 741–77.
[2] Kennedy LA, Bingue JP, Saveliev AV, Fridman AA, Foutko SI. Chemical structures of methane–air filtration combustion waves for fuel-lean and fuel-rich conditions. Proc Combust Inst 2000;28:1431–8.
[3] Dhamrat RS, Ellzey JL. Numerical and experimental study of the conversion of methane to hydrogen in a porous media reactor. Combust Flame 2006;144:698–709.
[4] Aguilar J, Fuentes R, Viramontes R. Simulation of iron ore reduction in a fixed bed. Model Simul Mater Sci Eng 1995;3:131–47.
[5] Parisi DR, Laborde MA. Modeling of counter current moving bed gas-solid reactor used in direct reduction of iron ore. Chem Eng J 2004;104:35–43.
[6] Takenaka Y, Kimura Y, Narita K, Kaneko D. Mathematical model of direct reduction shaft furnace and its application to actual operations of a model plant. Comput Chem Eng 1986;10:67–75.
[7] Alamsari B, Tori S, Trianto A, Bindar Y. Heat and mass transfer in reduction zone of sponge iron reactor. ISRN Mech Eng 2011:12. Article ID 324659.
[8] Mondal K, Lorethova H, Hippo E, Wiltowski T, Lalvani S. Reduction of iron oxide in carbon monoxide atmosphere - reaction controlled kinetics. Fuel Process Technol 2004;86:33–47.
[9] Valipour M. Mathematical modeling of a non-catalytic gas-solid reaction: hematite pellet reduction with syngas. Trans C: Chem Chem Eng 2009;16:108–24.
[10] Nouri S, Ebrahim HA, Jamshidi E. Simulation of direct reduction reactor by the grain model. Chem Eng J 2011;166:704–9.
[11] Levenspiel O. Chemical reaction engineering. 3rd ed. New York, NY, USA: John Wiley & Sons; 1999.
[12] Toledo M, Bubnovich V, Saveliev A, Kennedy L. Hydrogen production in ultrarich combustion of hydrocarbon fuels in porous media. Int J Hydrog Energy 2009;34:1818–27.
[13] Nield D, Bejan A. Convection in porous media. 3rd ed. New York: Springer; 2009.
[14] Fuller EN, Schettler PD, Giddings JC. New method for prediction of binary gas-phase diffusion coefficients. Industrial Eng Chem 1966;58:18–27.
[15] Bubnovich V, Toledo M. Analytical modelling of filtration combustion in inert porous media. Appl Therm Eng 2007;27:1144–9.
[16] Wakao N, Kaguei S. Heat and mass transfer in packed beds. New York: Gordon and Breach Science Publications; 1982.
[17] National Institute of Standards and Technology. From NIST 69: http://webbook.nist.gov/chemistry/
[18] Babkin V. Filtrational combustion of gases. Present state of affairs and prospects. Pure Appl Chem 1993;65:335–44.

Nomenclature

A_p: Pellet surface area, m^2
b: Stoichiometric coefficient
C_i: Molar concentration of specie i, mol/m^3
$C_{p,i}$: Specific heat of specie i, J/mol/K
$C_{p,s}$: Specific heat of the solid phase, J/kg/K
Co: Solid conversion, $kmol/m^3$
$\mathscr{D}_{e,i}$: Effective diffusivity of the gaseous reactant i, $i = CO, H_2$, m^2/s
$\mathscr{D}_{M,i-gas}$: Molecular diffusivity of the gaseous reactant i in gas, $i = CO, H_2$, m^2/s
D: Pellet diameter, M
d_c: Quartz tube diameter, M
h: Heat transfer coefficient, $W/m^2/K$
h_v: Volumetric convective heat transfer coefficient, $W/m^3/K$
k_i: Mass transfer coefficient between the solid particle and gaseous reactant i, $i = CO, H_2$, m/s
k_i'': First-order rate constant for the surface reaction of the gaseous reactant i, $i = CO, H_2$, m/s
M_g: Molecular weight of the gaseous phase, kg/kmol
M_i: Molecular weight of the specie i, kg/kmol
Met: Metallization degree
n_p: Number of pellets per unit of reactor volume, $1/m^3$
Nu: Nusselt number
P: Total pressure, kPa, atm
Pr: Prandtl number
$\dot{Q}_v$: Internal heat generation due to unconsidered reactions that occur in the gaseous phase, W/m^3
R: Pellet radius, M
Re: Reynolds number
r_c: Radius of the unreacted core, M
r_j: Rate of reaction j, kmol/s
t: Time, S
T_g: Temperature of the gaseous phase, K
T_0: Reference temperature, 298 [K], K
T_s: Temperature of the solid phase, K
u_g: Velocity of the gaseous phase, m/s
$V_{a,st}$: Stoichiometric volume of air needed to burn a kilogram of fuel at normal temperature and pressure conditions, Nm^3/kg fuel
$\dot{V}_{a,st}$: Stoichiometric air flow, m^3/s
X_{O_2}: Volume fraction of oxygen in air, m^3/m^3
y_i: Mass fraction of specie i in the fuel, $i = C, H$, kg/kg
z: Axial coordinate, m

Greek letters

ΔH_j: Heat of reaction j, kJ/mol
$\Delta H_{f,i}^{\circ}$: Standard enthalpy of formation of specie i, kJ/mol
$\Delta H_{red,i}$: Heat of the reduction reaction of Fe_2O_3 by $i, i = CO, H_2$, kJ/mol
β_v: Heat transfer coefficient to the surroundings, $W/m^3/K$
ε: Bed porosity, m^3/m^3
ε': Emissivity of the solid phase, $0 < \varepsilon' < 1$
ε'': Transmissivity of the solid phase, $0 < \varepsilon' < 1$
ζ: Adjustment factor for CO reaction
λ_{ef}: Effective thermal conductivity of the solid phase, W/m/K
λ_g: Thermal conductivity of the gaseous phase, W/m/K
λ_i: Thermal conductivity of specie i, W/m/K
λ_s: Thermal conductivity of the solid phase, W/m/K
ξ: Adjustment factor for H_2 reaction
ρ_g: Density of the gaseous phase, kg/m^3
ρ_i: Density of specie i, kg/m^3
ρ_s: Density of the solid phase, kg/m^3
$\sum \Delta H_j r_j$: Mathematical expression related to the heat of reactions (1) and (2), J/s
$\sum \overline{v}_i$: Sum of the diffusion volumes for specie i
σ: Stephan–Boltzmann constant, $5.67051 \cdot 10^{-8}$, $W/m^2/K^4$
φ: Equivalence ratio, m^3/m^3

Subscripts

a: Air
CH_4: Methane
CO: Carbon monoxide
CO_2: Carbon dioxide
f: Fuel
Fe: Metallic iron
Fe_2O_3: Hematite

g: Gaseous phase
H_2: Hidrogen
H_2O: Water vapor
i: Species index
j: Reactions index
s: Solid phase
0: Initial state

Superscripts

$^\circ$: Standard conditions, standard state
n: Time n regarding to the implicit finite differences scheme
$n+1$: Time n+1 regarding to the implicit finite differences scheme